N72-30922

NASA TECHNICAL NOTE

NASA TN D-6899

NASA TN D-6899

CASE FILE
COPY

FATIGUE CRACK GROWTH FROM A CIRCULAR HOLE WITH AND WITHOUT HIGH PRIOR LOADING

by John H. Crews, Jr., and N. H. White

Langley Research Center
Hampton, Va. 23365

NATIONAL AERONAUTICS AND SPACE ADMINISTRATION • WASHINGTON, D. C. • SEPTEMBER 1972

1. Report No.	2. Government Accession No.	3. Recipient's Catalog No.
NASA TN D-6899		

4. Title and Subtitle	5. Report Date
FATIGUE CRACK GROWTH FROM A CIRCULAR HOLE WITH AND WITHOUT HIGH PRIOR LOADING	September 1972
	6. Performing Organization Code
7. Author(s)	8. Performing Organization Report No.
John H. Crews, Jr., and N. H. White	L-8305
	10. Work Unit No.
9. Performing Organization Name and Address	501-22-02-01
NASA Langley Research Center Hampton, Va. 23365	11. Contract or Grant No.
	13. Type of Report and Period Covered
12. Sponsoring Agency Name and Address	Technical Note
National Aeronautics and Space Administration Washington, D.C. 20546	14. Sponsoring Agency Code

15. Supplementary Notes

16. Abstract

Fatigue crack growth from a circular hole was investigated experimentally and analytically. An aluminum-alloy sheet specimen was cycled under a single level of loading with and without prior high loads. Tests showed that the crack propagation life was significantly longer when the high loads were applied initially. This longer life was attributed to compressive residual stresses produced near the hole by the initial high loads.

The residual stresses near the hole were determined by an elastoplastic analysis and were then used to develop a stress-intensity solution for a crack growing through the residual stress field. This solution and a similar solution for the case of no prior loading were used to predict crack growth. The predicted crack growth agreed closely with the experimental values.

17. Key Words (Suggested by Author(s))	18. Distribution Statement
Crack propagation Stress concentration Stress-intensity factors High prior loading Residual stress	Unclassified – Unlimited

19. Security Classif. (of this report)	20. Security Classif. (of this page)	21. No. of Pages	22. Price*
Unclassified	Unclassified	33	$3.00

*For sale by the National Technical Information Service, Springfield, Virginia 22151

FATIGUE CRACK GROWTH FROM A CIRCULAR HOLE WITH AND WITHOUT HIGH PRIOR LOADING

By John H. Crews, Jr., and N. H. White
Langley Research Center

SUMMARY

Fatigue crack growth from a circular hole was investigated experimentally and analytically. An aluminum-alloy sheet specimen was cycled under a single level of loading with and without prior high loads. Tests showed that the crack propagation life was significantly longer when the high loads were applied initially. This longer life was attributed to compressive residual stresses produced near the hole by the initial high loads.

The residual stresses near the hole were determined by an elastoplastic analysis and were then used to develop a stress-intensity solution for a crack growing through the residual stress field. This solution and a similar solution for the case of no prior loading were used to predict crack growth. The predicted crack growth agreed closely with the experimental values.

INTRODUCTION

Fatigue life can be predicted on the basis of crack propagation alone (refs. 1 and 2). A small initial crack is assumed to exist, and the time required to propagate this crack to a critical length is calculated and assumed equal to fatigue life. This approach involves certain practical complexities when applied for structures. First, since fatigue cracks usually initiate at stress concentrations that cause high local stresses, the influence of local stress must be accounted for. Second, since localized yielding often precedes crack initiation and alters local stresses, it must also be accounted for. The purpose of the present study is to demonstrate the influence of local stresses on crack propagation and to present a method for incorporating this influence into crack-propagation predictions.

The problem studied was that for 2024-T3 aluminum-alloy sheet specimens containing a circular hole for two cases of uniaxial loading. Both cases involved constant-amplitude loading at a level that produced elastic stresses near the hole, but in one case this loading was preceded by several applications of a high load. This prior loading yielded the material near the hole; residual stresses were produced which altered the distribution of the subsequent elastic stresses near the hole.

The influence of local stress distribution on crack growth was investigated by conducting tests with the two types of loading. Local stresses were calculated for an uncracked sheet specimen for each of the two cases of loading and were then used in an analysis of stress-intensity factors for cracks extending from the hole. The crack lengths beyond which the influence of the hole can be neglected were determined for each type of loading. To account for nonuniform stresses along the plane of the crack, growth predictions were made by a stress-intensity procedure like that used in references 3 and 4. The predicted and measured crack-growth results were compared to evaluate the analytical procedures.

SYMBOLS

The units used for the physical quantities defined in this paper are given both in the International System of Units (SI) (ref. 5) and in the U.S. Customary Units. The measurements and calculations were made in the U.S. Customary Units.

A_n, B_n arbitrary constants

a crack length relative to center of specimen, mm (in.)

b dimension locating concentrated force, mm (in.)

C,m material crack-growth constants

E Young's modulus, MN/m^2 (ksi)

E_s secant modulus, MN/m^2 (ksi)

i,n indices

K stress-intensity factor, $MN/m^{3/2}$ $\left(ksi\ \sqrt{in.}\right)$

K_b component of stress-intensity factor corresponding to boundary collocation, $MN/m^{3/2}$ $\left(ksi\ \sqrt{in.}\right)$

K_c critical stress-intensity factor

K_f component of stress-intensity factor corresponding to concentrated forces on crack, $MN/m^{3/2}$ $\left(ksi\ \sqrt{in.}\right)$

K_T	elastic stress-concentration factor
K_ϵ	strain-concentration factor
K_σ	stress-concentration factor
L	crack length relative to edge of hole, mm (in.)
M,J	limits for indices
N	crack-propagation period, cycles
P	concentrated force, N (lb)
R	ratio of minimum to maximum stress
r,θ	polar coordinates, mm (in.), deg
S	gross section nominal stress, MN/m^2 (ksi)
t	specimen thickness, mm (in.)
w	specimen width, mm (in.)
x,y	Cartesian coordinates, mm (in.)
Z_1	Westergaard stress function
z	complex variable, $x + iy$
α	correction factor for finite width
ΔK	range of stress-intensity factor, $MN/m^{3/2}$ $\left(ksi\sqrt{in.}\right)$
ρ	radius of circular hole, mm (in.)
σ	local stress, MN/m^2 (ksi)
$\overline{\sigma}$	effective stress, MN/m^2 (ksi)

$\bar{\sigma}_e$ elastic effective stress, MN/m^2 (ksi)

$\sigma_r, \tau_{r\theta}$ normal and shear stress components in polar coordinates, MN/m^2 (ksi)

σ_x, σ_y normal stress components in Cartesian coordinates, MN/m^2 (ksi)

σ_{xe}, σ_{ye} elastic normal stress components in Cartesian coordinates, MN/m^2 (ksi)

$\phi(z), \Omega(z)$ Muskhelishvili stress functions

Subscript:

max maximum

TEST PROCEDURE AND RESULTS

Specimen and Loading

The specimen configuration and dimensions are shown in figure 1. Sheet 2024-T3 aluminum alloy was used with the sheet-rolling direction parallel to the applied cyclic loading. Fatigue cracks developed at the boundary of the hole and propagated along the transverse axis.

The two loading sequences used in this study are shown in figure 2. The single-level loading (R = 0, S = 115 MN/m^2 (16.7 ksi)) in figure 2(a) was selected to produce only elastic stresses (it therefore established the basic influence of the hole on the initial stage of crack growth). In contrast, the high load (R = -1, S = 230 MN/m^2 (33.3 ksi)) in the two-level sequence shown in figure 2(b) was selected to produce local yielding and the concomitant residual stresses near the hole. The high load cycling was terminated after the tenth positive half-cycle; the second loading level in the two-level sequence was identical to that in figure 2(a).

Test Procedure

The specimens were tested in an axial-load testing machine which operated at two frequencies, 0.25 Hz and 13.3 Hz. They were cyclically loaded at 13.3 Hz during the slow initial stage of crack growth; later they were loaded at 0.25 Hz during the higher growth rates. The prior high loads were applied manually.

Fatigue cracks started at the boundary of the hole after 120 000 and 460 000 cycles, respectively, for the single-level and two-level loading sequences. These cracks were

detected and measured through a 10-power microscope. A scale was taped to the specimen for a reference. As shown in figure 3(a), crack length was referenced to the center of the hole by length a or to the edge of the hole by length L. An initial length of $L = 0.76$ mm (0.03 in.) was defined as the beginning of the crack-propagation period; crack-growth data were recorded beyond this initial length.

Six tests were conducted, three for each of the two types of loading. To simplify the analysis, symmetrical crack growth was desired; but in every test a fatigue crack started only on one side of the hole. Inasmuch as the difference between stress-intensity factors for a single crack from a hole and symmetrical cracks is less than 5 percent when the cracks are shorter than $L = 3.8$ mm (0.15 in.) (ref. 6), the crack was allowed to grow to this length before the opposite side of the hole was slit to the same length to promote symmetrical crack growth. When each test was continued, a crack quickly appeared at the end of the slit and the cracks grew symmetrically.

Test Results

Observation of fracture surfaces revealed that in all tests the cracks started at the intersection of the sheet face and the hole; the cracks then extended radially as shown in figure 3(b). This so-called corner-crack configuration was maintained until the crack extended through the thickness. A similar crack-growth sequence was reported in reference 7.

Test data are presented in table 1 and also in figure 4 for crack length L and crack-propagation period N. Average crack-propagation periods were 5200 cycles for the single-level loading and 31 000 cycles for the two-level loading. These results are analyzed in the following section.

ANALYSIS

A procedure was presented in reference 3 for predicting crack growth through a nonuniform stress field. Those predictions, which were for cracks growing near simulated rivet forces, were based on calculated stress-intensity factors and a so-called K-rate curve which related experimental crack-growth rates to stress-intensity factors. A similar procedure was used in the present study to predict crack growth through the nonuniform stress field near the circular hole. The approach involved three steps: first, calculation of the stress distribution near the hole, second, calculation of the stress intensity factors for cracks in and through the local stress field, and finally, prediction of the crack growth based on the stress-intensity solution and a K-rate curve.

Stress Distributions

The stresses of interest are those along the transverse axis of the central-hole specimen before the crack was initiated. The general procedures used to calculate these stresses are described in appendix A.

For the case of single-level loading, the conditions were elastic; as discussed in appendix A, the elastic stress σ_{ye} on the transverse axis is given by

$$\sigma_{ye} = \frac{S}{2}\left[2 + \left(\frac{\rho}{x}\right)^2 + 3\left(\frac{\rho}{x}\right)^4\right] \tag{1}$$

Equation (1) is plotted as the lower solid curve in figure 5. Because the loading produced only elastic stresses, no residual stresses remained after the specimen was unloaded. Stresses therefore alternated between the values given by the solid curve and zero.

For the case of two-level loading, the initial high loads produced yielding near the hole. The resultant elastoplastic stresses were determined by first calculating the stresses with elastic theory and then correcting these stresses to account for the local yielding, as explained in appendix A. The distribution of elastic stresses σ_{ye} for the high load was obtained from equation (1) and is shown as the upper solid curve in figure 5. The corresponding elastoplastic stresses σ_y were found from

$$\sigma_y = \sigma_{ye}\sqrt{\frac{E_s}{E}} \tag{2}$$

where E_s is the secant modulus and E is the Young's modulus. The dash-dot curve represents the stress distribution corrected for yielding. Since yielding reduced the stresses within the plastic zone, the elastic stresses outside the zone must be increased to maintain equilibrium; this was accomplished by raising the elastic curve as shown in figure 5.

The high loads in the two-level sequence produced cyclic strain hardening, typical of 2024-T3 aluminum alloy; however, results in reference 8 show that 10 cycles of this loading are sufficient to stabilize the hardening. (This was actually the basis for selecting 10 cycles of high load in the present investigation.) The dash-dot curve in figure 5 represents stresses for the last cycle of high load and was calculated by using values of E_s from the stabilized cyclic stress-strain curve in reference 8.

During unloading from the last high load, the material yielded in compression in a very localized region near the hole. For this region, stresses were calculated by again using equation (2) and the procedure in appendix A. Stresses outside this region were calculated by elasticity theory. The resulting distribution of residual stress after high loading is shown as the lower dashed curve in figure 5.

Since the low loads in the two-level sequence produced only elastic stresses, the stresses produced by these loads were found by adding the elastic-stress ranges from equation (1) to the residual stresses. The maximum stresses for low loads are shown by the upper dashed curve in figure 5. For subsequent load cycles, the stress cycled between the two dashed curves.

Although the low loads in the two-level sequence were identical to those for the single-level sequence, the local stresses near the hole are quite different for the two sequences. Comparison of the lower solid curve and the upper dashed curve for single- and two-level loading, respectively, shows this difference to be as large as 200 MN/m^2 (30 ksi). The influence of local stresses on crack growth is discussed in the following section in terms of stress-intensity factors.

Stress-Intensity Factors

As previously mentioned, all cracks started at the intersection of the sheet face and the hole (corner-crack configuration). Because of difficulties in analyzing a corner crack in a finite-thickness sheet, the initial crack (0.76 mm (0.03 in.)) was assumed to have a straight front which extended through the complete sheet thickness. Stress-intensity factors for this assumed configuration were calculated by a procedure described in appendix B.

Maximum stress-intensity factors are presented in table 2 for a range of normalized crack lengths. Stress-intensity factors for the single-level loading are presented in figure 6 for comparison with Bowie's solution (ref. 6). The two curves agree very closely for small crack lengths and deviate only slightly for long crack lengths. This close correlation substantiates the procedures described in appendix B.

The influence of the hole on crack growth can be examined by comparing stress-intensity factors for the reference case of a cracked sheet without a hole with those from the present study. (See fig. 7.) For the case of single-level loading (solid curve), stress-intensity values rapidly approach the reference curve for a cracked sheet without a hole; for L/ρ larger than about 0.2, they deviate from this curve by less than ± 5 percent. Therefore, for L/ρ larger than 0.2 the influence of the hole can be neglected. However, since stress-intensity factors are initially very small, a large percentage of the crack-propagation period is spent in growing the crack to a length of $L/\rho = 0.2$ – about 70 percent for single-level loading (table 1).

For the case of two-level loading (dashed curve in fig. 7), comparison with the reference curve (dash-dot curve) shows that the influence of the hole exists for larger crack lengths than for single-level loading; the stress intensity is within ± 5 percent of the reference case for L/ρ larger than about 0.5. To grow the crack to $L/\rho = 0.5$ took about 95 percent of the crack-propagation period. For large crack lengths the solution for two-

level loading deviates from the reference curve, probably because of the manner in which stress redistribution due to yielding was approximated. However, since only 5 percent of the crack-propagation period remained beyond $L/\rho = 0.5$, this apparent error in stress intensity for long cracks was not expected to seriously influence the predictions.

Prediction of Crack Growth

The K-rate curve for 2024-T3 aluminum alloy was established in the present study by measuring crack-growth rates in centrally cracked specimens under constant-amplitude, $R = 0$ loading. These specimens were of the same size and thickness as the specimens with a central hole. The range of stress intensity for this case is given by

$$\Delta K = S_{max}\sqrt{\pi a}\,\alpha$$

where α is a finite-width correction which was required because cracks were grown to aspect ratios (2a/w) up to 0.75. This correction (ref. 9) is

$$\alpha = \sqrt{\sec \frac{\pi a}{w}} \tag{3}$$

Measured crack-growth rates as a function of stress-intensity range are shown in figure 8.

The following empirical equation (ref. 10) has been shown to accurately represent K-rate data:

$$\frac{da}{dN} = \frac{C(\Delta K)^m}{(1 - R)K_c - \Delta K} \tag{4}$$

where K_c is critical-stress intensity at fracture and C and m are material constants. These constants were evaluated for the data in figure 8. The solid curve represents a least-squares fit for the data; the dashed curves bracket 90 percent of the data.

Predictions for crack growth from the circular hole were based on the following procedure: first, the stress-intensity values were taken from table 2 for increments of crack length; second, these values were corrected with equation (3) to account for finite specimen width; third, the corrected stress-intensity values were used in equation (4) to calculate the corresponding crack-growth rates; and finally, the crack length and number of cycles were determined by numerical integration.

The crack-growth predictions for single-level loading are shown in figure 9; the solid curve is based on the mean K-rate curve and the dashed curves are based on the 90-percent-data scatter limits from figure 8. The predicted range for the crack growth

brackets the experimental results. This close correlation substantiates the prediction procedure.

Crack-growth predictions for two-level loading cannot be based on the zero-to-tension (R = 0) K-rate curve (fig. 8) since the local stresses were found to cycle between compression and tension near the hole (see fig. 5). In fact, these local stresses cannot be characterized by a single R value – for very small cracks the local stress ratio is nearly R = -1, but for longer cracks it approaches R = 0. This problem was dealt with by two approximate approaches for predicting the crack growth.

For the first approach, the compressive portion of the local-stress cycle was neglected, to be consistent with the zero-to-tension K-rate curve. The necessary stress-intensity ranges were taken directly from table 2. For the second approach, the compressive residual stresses were assumed equal in magnitude to the tensile stresses; that is, the local stresses were assumed to be completely reversed (R = -1). This approach was considered because the experimental results show that a large portion of the crack-growth period was spent while the cracks were quite small, and, as previously mentioned, the stress field surrounding a small crack consists of nearly completely reversed local stresses. Crack growth was predicted using a K-rate curve for R = -1 loading (ref. 11); stress-intensity ranges were determined by simply doubling the values in table 2.

Predictions based on these two approaches are shown in figure 9. As expected, the first approach predicted a crack-growth period (solid curve) that is larger than those found experimentally; for the material used in this study, the compressive portion of the stress cycle has been shown to contribute to crack growth (ref. 11). The dashed curves bracketing the solid curve are based on the 90-percent-data scatter limits from figure 8. The second approach predicted the dash-dot curve which agrees quite well with experimental results. Since reference 11 did not contain information on scatter, the scatter band about the dash-dot curve has been omitted.

CONCLUDING REMARKS

Fatigue crack growth from a circular hole has been investigated analytically and experimentally with 2024-T3 aluminum-alloy sheet specimens. Two types of tests were performed; both involved constant-amplitude loading at a level that produced elastic stresses near the hole, but for one type of test this loading was preceded by several applications of a high load which produced yielding near the hole.

The prior high loads significantly lengthened the crack-propagation period. This effect was attributed to compressive residual stresses produced around the hole.

The stress distributions near the hole were determined by an elastoplastic analysis and were used to calculate stress-intensity factors. As expected, stress-intensity factors

were smaller for the case involving high prior loading. The stress-intensity solutions were used to predict crack growth from the hole. Although several simplifying assumptions were involved, the predicted growth was in good agreement with measured results.

Stress-intensity factors also illustrated the very localized influence of the hole on crack behavior. Stress-intensity factors for symmetrical cracks growing from a hole became equal to those for a central crack at rather short crack lengths: 0.2 and 0.5 times the hole radius for the cases of no prior loading and high prior loading, respectively. After escaping the influence of the hole, a crack may be assumed to be equivalent to a center crack with a half-length equal to the hole radius plus the crack length.

Although the influence of the hole was quite localized, its effect on crack propagation operated for a large portion of the crack-propagation period – 70 percent of the period for no high initial loading and 95 percent of the period for high initial loading. Since fatigue cracks in structures typically originate at stress concentrations, such as holes, these results emphasize the need for improved fatigue-prediction methods which accurately model crack growth from holes.

Langley Research Center,
National Aeronautics and Space Administration,
Hampton, Va., August 11, 1972.

APPENDIX A

STRESS DISTRIBUTIONS NEAR A CIRCULAR HOLE

Elastic Loading

For elastic stresses, the solution in reference 12 for a hole in a finite sheet is directly applicable. However, the solution for an infinite sheet is much simpler and is sufficiently accurate for the wide plate used in this study. For the infinite-width configuration, the desired stress σ_{ye} on the transverse axis is given (see, for example, ref. 13) by

$$\sigma_{ye} = \frac{S}{2}\left[2 + \left(\frac{\rho}{x}\right)^2 + 3\left(\frac{\rho}{x}\right)^4\right] \tag{A1}$$

This equation was used to calculate local stresses for the constant-amplitude loading in the present study.

Inelastic Loading

The high-load cycles in the two-level sequence in the present study produced localized yielding near the hole. The resultant elastoplastic stresses were calculated by a procedure presented in reference 14. In this procedure the stresses are calculated by elastic theory, then corrected to account for yielding and the biaxial stress state near the hole.

The desired elastoplastic y-component of stress σ_y on the transverse axis can be expressed as

$$\sigma_y = \sigma_{ye}\sqrt{\frac{E_s}{E}} \tag{A2}$$

where σ_{ye} is the stress from elasticity theory, E_s is the secant modulus, and E is the Young's modulus. It should be noted that although equation (A2) was developed in reference 14 for stresses near a crack tip, it can also be derived from the well-known Neuber equation for notches: $K_T^2 = K_\sigma K_\epsilon$ when K_σ and K_ϵ are stress and strain concentration factors, respectively (ref. 15). The σ_{ye} in equation (A2) can be determined directly from equation (A1); but the E_s in equation (A2) cannot be established by a simple direct method because E_s is a function of σ_y in this equation. For the present study E_s was found by a graphical procedure described in the remainder of this section.

Because the biaxial-stress state near the hole increases the stress required for a given strain to a value above that for the uniaxial-stress state, the stress from a uniaxial

stress-strain curve must be adjusted. The adjusted stress was called the effective stress $\bar{\sigma}$ which for the transverse axis can be expressed as

$$\bar{\sigma} = \sqrt{\sigma_x^2 - \sigma_x\sigma_y + \sigma_y^2} \tag{A3}$$

where σ_x is the x-component of stress. Using the format of equation (A2) to express σ_x and σ_y, equation (A3) becomes

$$\bar{\sigma} = \bar{\sigma}_e\sqrt{\frac{E_s}{E}} \tag{A4}$$

where $\bar{\sigma}_e$ is the elastic effective stress given by

$$\bar{\sigma}_e = \sqrt{\sigma_{xe}^2 - \sigma_{xe}\sigma_{ye} + \sigma_{ye}^2} \tag{A5}$$

The σ_{ye} can be determined from elasticity theory by using equation (A1); σ_{xe} can be determined by using the following equation (ref. 13)

$$\sigma_{xe} = \frac{3S}{2}\left[\left(\frac{\rho}{\bar{x}}\right)^2 - \left(\frac{\rho}{\bar{x}}\right)^4\right] \tag{A6}$$

The stress along the transverse axis was determined by using the preceding equations together with the stress-strain curve according to the following steps:

(1) For given values of S and x, σ_{xe} and σ_{ye} were calculated from equations (A6) and (A1), respectively.

(2) These values of σ_{xe} and σ_{ye} were used in equation (A5) to calculate $\bar{\sigma}_e$.

(3) The value of $\bar{\sigma}_e$ was substituted into equation (A4) and this equation was plotted as in figure 10.

(4) Values of E_s/E, and σ (uniaxial stress) were taken from a stress-strain curve for the material and were also plotted in figure 10.

(5) The intersection of these two curves, point A in figure 10, represents a solution to equation (A4) consistent with the material stress-strain reponse. The value of E_s/E for point A is the desired value corresponding to $\bar{\sigma}$. This value of E_s/E was therefore substituted into equation (A2) to determine σ_y. The procedure was repeated for a range of x-values to obtain the distribution of σ_y on the transverse axis.

This procedure is equally applicable for the unloading portion of an applied load cycle. For this case, the curve of E_s/E against σ is derived from a stress-strain

curve for unloading from a plastic stress-strain state (see ref. 8). The dashed curve in figure 10 was derived in this manner and was used with equation (A4) to determine point B, a typical graphical solution for E_s/E and $\bar{\sigma}$ for unloading. Stress after unloading was found by subtracting the unloading stress range from the maximum stress immediately before unloading.

APPENDIX B

STRESS-INTENSITY FACTORS

Stress-intensity factors were sought for an axially loaded sheet containing two symmetrical cracks emanating from a circular hole. For simplicity, an infinite width was assumed. A stress-intensity solution exists (ref. 6) for this infinite-width case and is directly applicable to the case of single-level loading used in the present study. But, for the case of two-level loading, the stress distribution near the hole is complex; no solution for this distribution exists. For this reason a solution was developed for an arbitrary stress distribution, then specialized for the stress distributions corresponding to the single-level and two-level loading cases.

The analysis was based on a superposition of loads that permitted the case under study to be analyzed in terms of two tractable loading cases. This superposition is represented in figure 11. In part (a) the sheet is loaded by a remote tensile stress S and by a stress $\sigma(x)$ acting on the crack surface. This $\sigma(x)$, which tends to close the crack, was taken equal to that which exists along the x-axis for an uncracked sheet with a hole. The stress acting on the crack in part (b) is equal but opposite to $\sigma(x)$ in part (a). Superposition of parts (a) and (b) causes the stresses on the crack to cancel one another and produces the desired stress-free crack with remote loading shown in part (c).

Since $\sigma(x)$ is equal to the stress in an uncracked sheet when $\sigma(x)$ is applied to the crack surface as in part (a), the crack is effectively eliminated; part (a) therefore represents an uncracked sheet with a hole. As a result, the stress-intensity factors sought for part (c) are those operative in part (b).

The stress-intensity analysis of part (b) consisted of two phases: first, stress-intensity factors were found for $-\sigma(x)$ acting on a central crack in a sheet without a hole; then, the influence of the hole was introduced as an additional component of stress intensity. This procedure is briefly described in the following sections.

Discretization of Stress Distributions on the Crack Surfaces

The stress distribution $-\sigma(x)$ along the crack surface was simulated by applying concentrated forces at 0.0635-mm (0.0025-in.) intervals. The resulting system of forces was analyzed by considering sets of four symmetrically located forces P_i, as shown in figure 12(a). The stress-intensity factor K_i for each set of forces was given in reference 16 as

$$K_i = \frac{2P_i\sqrt{\pi a}}{\pi t\sqrt{a^2 - b_i^2}}$$

The stress-intensity factor for the complete system of M-forces, figure 12(b), was found by summing the stress-intensity factor corresponding to each set of forces as follows:

$$K_f = \sum_{i=1}^{M} \frac{2P_i\sqrt{\pi a}}{\pi t\sqrt{a^2 - b_i^2}} \tag{B1}$$

Boundary Collocation for a Circular Hole

The influence of the hole was introduced by eliminating stress along the circular arc $\rho = 1$ by boundary collocation. Normal and tangential stresses along this arc were found for each set of forces and were summed to determine the stresses that must be eliminated to produce a stress-free boundary. Stresses were based on the Westergaard stress function (ref. 17)

$$Z_1(z) = \frac{2P_i z\sqrt{\pi}}{\pi t\left(z^2 - b_i^2\right)}\left(\frac{a^2 - b_i^2}{z^2 - a^2}\right)^{1/2}$$

and were expressed as

$$\sigma_r = \left(\text{Re } Z_1 - y \text{ Im } Z_1'\right)\cos^2\theta + \left(\text{Re } Z_1 + y \text{ Im } Z_1'\right)\sin^2\theta$$

$$- 2y \text{ Re } Z_1 \sin\theta\cos\theta \tag{B2}$$

and

$$\tau_{r\theta} = y\left[2 \text{ Im } Z_1'\sin\theta\cos\theta - \text{Re } Z_1'\left(\cos^2\theta - \sin^2\theta\right)\right] \tag{B3}$$

The boundary-collocation stresses were expressed in terms of the following complex stress functions presented in reference 18:

$$\phi(z) = \sum_{n=1}^{J}\left(\frac{A_n}{z^{2n-1}\sqrt{z^2 - a^2}} + \frac{B_n}{z^{2n}}\right)$$

and

$$\Omega(z) = \sum_{n=1}^{J} \left(\frac{A_n}{z^{2n-1}\sqrt{z^2 - a^2}} - \frac{B_n}{z^{2n}} \right)$$

Separation of real and imaginary parts in

$$\sigma_r - i\tau_{r\theta} = \phi(z) + \overline{\phi(z)} - \left[(\bar{z} - z)\phi'(z) - \phi(z) + \overline{\Omega}(z) \right] e^{2i\theta}$$

leads to

$$\sigma_r = \sum_{n=1}^{J} \left(2A_n \left\{ \frac{1}{r^{2n-1}\sqrt{r_1 r_2}} \cos\left[(2n - 1) + \beta_1 \right] - \frac{(2n - 1)y}{r^{2n}\sqrt{r_1 r_2}} \sin\left[(2n - 2) + \beta_1 \right] \right.\right.$$

$$\left.\left. - \frac{y}{r^{2n-2}\sqrt{(r_1 r_2)^3}} \sin\left[(2n - 4)\theta + \beta_2 \right] \right\} + 2B_n \left[\frac{1}{r^{2n}} \cos 2n\theta \right.\right.$$

$$\left.\left. - \frac{2ny}{r^{2n+1}} \sin(2n - 1)\theta + \frac{1}{r^{2n}} \cos(2n - 2)\theta \right] \right) \qquad \text{(B4)}$$

and

$$\tau_{r\theta} = \sum_{n=1}^{J} \left(2A_n \left\{ \frac{(2n - 1)y}{r^{2n}\sqrt{r_1 r_2}} \cos\left[(2n - 2) + \beta_1 \right] + \frac{y}{r^{2n-2}\sqrt{(r_1 r_2)^3}} \cos\left[(2n - 4)\theta + \beta_2 \right] \right\} \right.$$

$$\left. + 2B_n \left[\frac{2ny}{r^{2n+1}} \cos(2n - 1)\theta + \frac{1}{r^{2n}} \sin(2n - 2)\theta \right] \right) \qquad \text{(B5)}$$

where

$$r \equiv \sqrt{x^2 + y^2} \qquad \theta \equiv \tan^{-1}\left(\frac{y}{x}\right) \qquad \beta_1 \equiv \frac{1}{2}\left(\theta_1 + \theta_2\right)$$

$$r_1 \equiv \sqrt{(x - a)^2 + y^2} \qquad \theta_1 \equiv \tan^{-1}\left(\frac{y}{x - a}\right) \qquad \beta_2 \equiv \frac{3}{2}\left(\theta_1 + \theta_2\right)$$

$$r_2 \equiv \sqrt{(x + a)^2 + y^2} \qquad \theta_2 \equiv \tan^{-1}\left(\frac{y}{x + a}\right)$$

Stresses from pairs of equations (B2), (B4) and (B3), (B5) were added at J-points along the circular arc to satisfy the conditions $\sigma_r = \tau_{r\theta} = 0$ at each point. The resulting set of 2J-equations was solved for A_n and B_n. The stress-intensity factor corresponding to the boundary-collocation stresses was written in terms of $\phi(z)$, according to reference 16, as

$$K_b = 2\sqrt{2\pi} \lim_{z \to a} \sqrt{z - a}\, \phi(z) \tag{B6}$$

The stress-intensity factor for the case in figure 12(b) was written as the sum of the contributions from equations (B1) and (B6) to give

$$K = \sum_{i=1}^{M} \frac{2P_i\sqrt{\pi a}}{\pi t\sqrt{a - b_i^2}} + 2\sqrt{2\pi} \lim_{z \to a} \sqrt{z - a}\, \phi(z) \tag{B7}$$

This is the desired stress-intensity equation for the configuration and loading in the present study.

REFERENCES

1. Tiffany, C. F.; and Masters, J. N.: Applied Fracture Mechanics. Fracture Toughness Testing and Its Applications, Spec. Tech. Publ. No. 381, Amer. Soc. Testing Mater., 1965, pp. 249-278.

2. Sanga, R. V.; and Porter, T. R.: Application of Fracture Mechanics for Fatigue Life Prediction. Proceedings of the Air Force Conference on Fatigue and Fracture of Aircraft Structures and Materials, H. A. Wood, R. M. Bader, W. J. Trapp, R. F. Hoener, and R. C. Donat, eds., AFFDL TR 70-144, U.S. Air Force, 1970, pp. 595-610.

3. Figge, I. E.; and Newman, J. C., Jr.: Fatigue Crack Propagation in Structures With Simulated Rivet Forces. Fatigue Crack Propagation, Spec. Tech. Publ. No. 415, Amer. Soc. Testing Mater., 1967, pp. 71-93.

4. Poe, C. C., Jr.: Fatigue Crack Propagation in Stiffened Panels. Damage Tolerance in Aircraft Structures, Spec. Tech. Publ. No. 486, Amer. Soc. Testing Mater., 1971, pp. 79-97.

5. Comm. on Metric Pract.: ASTM Metric Practice Guide. NBS Handbook 102, U.S. Dep. Com., Mar. 10, 1967.

6. Bowie, O. L.: Analysis of an Infinite Plate Containing Radial Cracks Originating at the Boundary of an Internal Circular Hole. J. Math. & Phys., vol. XXXV, no. 1, Apr. 1956, pp. 60-71.

7. Schijve, J.; and Jacobs, F. A.: Fatigue Crack Propagation in Unnotched and Notched Aluminum Alloy Specimens. NLR-TR M.2128, Nat. Aero-Astronaut. Res. Inst. (Amsterdam), May 1964.

8. Crews, John H., Jr.: Elastoplastic Stress-Strain Behavior at Notch Roots in Sheet Specimens Under Constant-Amplitude Loading. NASA TN D-5253, 1969.

9. Brown, William F.; and Srawley, John E.: Plane Strain Crack Toughness Testing of High Strength Metallic Materials. Spec. Tech. Publ. No. 410, Amer. Soc. Testing Mater., c.1966, p. 78.

10. Forman, R. G.; Kearney, V. E.; and Engle, R. M.: Numerical Analysis of Crack Propagation in Cyclic-Loaded Structures. Trans. ASME, Ser. D: J. Basic Eng., vol. 89, no. 3, Sept. 1967, pp. 459-464.

11. Hudson, C. Michael: Effect of Stress Ratio on Fatigue-Crack Growth in 7075-T6 and 2024-T3 Aluminum-Alloy Specimens. NASA TN D-5390, 1969.

12. Howland, R. C. J.: On the Stresses in the Neighborhood of a Circular Hole in a Strip Under Tension. Phil. Trans. Roy. Soc. (London), ser. A, vol. 229, no. 671, Jan. 6, 1930, pp. 49-86.

13. Sokolnikoff, I. S.: Mathematical Theory of Elasticity. Second ed., McGraw-Hill Book Co., Inc. 1956, p. 291.

14. Dixon, J. R.; and Strannigan, J. S.: Strain Distributions Around Cracks in Ductile Sheets During Loading and Unloading. J. Mech. Eng. Sci., vol. 7, no. 3, Sept. 1965, pp. 312-317.

15. Neuber, H.: Theory of Stress Concentration for Shear-Strained Prismatical Bodies With Arbitrary Nonlinear Stress-Strain Law. Trans. ASME, Ser. E: J. Appl. Mech., vol. 28, no. 4, Dec. 1961, pp. 544-550.

16. Paris, Paul C.; and Sih, George C.: Stress Analysis of Cracks, Fracture Toughness Testing and Its Applications. Spec. Tech. Publ. No. 381, Amer. Soc. Testing Mater., c.1965, pp. 30-83.

17. Irwin, G. R.: Analysis of Stresses and Strains Near the End of a Crack Traversing a Plate. Trans. ASME, Ser. E: J. Appl. Mech., vol. 24, no. 3, Sept. 1957, pp. 361-364.

18. Newman, J. C., Jr.: An Improved Method of Collocation for the Stress Analysis of Cracked Plates With Various Shaped Boundaries. NASA TN D-6376, 1971.

TABLE 1.- CRACK PROPAGATION DATA

Crack length, L		Crack-propagation period, N, cycles					
mm	in.	Single-level loading			Two-level loading		
0.76	0.03	0	0	0	0	0	0
1.02	.04	978	1003	452	3 900	9 000	19 000
1.27	.05	1310	1675	1060	6 400	17 900	21 200
1.52	.06	1660	2185	1787	9 200	24 800	24 400
1.78	.07	1832	2550	2425	11 600	26 400	27 200
2.03	.08	1932	2760	2557	13 200	-----	28 800
2.29	.09	2009	3012	2891	-----	28 100	29 900
2.54	.10	2069	3214	3545	15 500	-----	31 000
3.05	.12	2172	3424	3910	17 100	29 400	32 700
3.56	.14	2246	3574	4083	18 300	30 200	33 500
4.06	.16	2300	3664	4369	18 900	30 800	34 041
4.57	.18	----	3730	4499	19 233	31 100	34 452
5.08	.20	2416	3790	4595	19 453	31 400	34 768
5.59	.22	2444	3860	----	19 614	31 600	34 992
6.10	.24	2499	3937	----	19 800	31 700	35 147
6.60	.26	2556	3983	----	19 937	31 900	35 286
7.11	.28	2601	4033	----	20 033	-----	35 418
7.62	.30	2647	4073	4873	20 104	32 100	35 552
10.15	.40	2827	4251	5051	20 523	32 438	35 992
12.70	.50	2973	4407	5189	20 810	32 693	36 304
15.24	.60	3116	4538	5312	21 055	32 857	36 532
17.78	.70	3222	4652	5438	21 190	33 014	36 752
20.32	.80	3323	4758	5541	21 314	33 130	36 932
22.86	.90	3410	4850	5634	21 412	33 226	37 049
25.40	1.00	3491	4923	5711	21 497	33 305	37 164
30.48	1.20	3611	5055	----	21 621	33 443	37 357
35.56	1.40	3704	5153	----	21 711	33 530	37 502
40.64	1.60	3776	5225	----	21 772	33 607	37 612
45.72	1.80	3826	5274	----	21 809	33 657	37 691
50.80	2.00	3858	5313	6162	21 836	33 694	37 746
55.88	2.20	3880	5338	----	-----	33 720	-----
60.96	2.40	3897	5354	----	-----	33 736	-----
66.04	2.60	3905	5364	----	21 858	33 746	-----
71.12	2.80	----	5367	----	-----	33 750	-----
76.20	3.00	----	----	6263	-----	-----	-----

TABLE 2.- MAXIMUM STRESS-INTENSITY FACTORS

[For symmetrical cracks extending from a circular hole in an infinite sheet]

Normalized crack length, L/ρ	Single-level loading				Two-level loading (low level)	
	Equation (B7)		Reference 6 (Bowie)			
	$MN/m^{3/2}$	$ksi\text{-}in^{1/2}$	$MN/m^{3/2}$	$ksi\text{-}in^{1/2}$	$MN/m^{3/2}$	$ksi\text{-}in^{1/2}$
0	0	0	0	0	0	0
.01	11.63	10.58	----	----	4.77	4.34
.02	12.01	11.84	----	----	5.25	4.77
.03	15.60	14.20	----	----	6.31	5.74
.04	18.08	16.45	----	----	7.48	1.77
.06	22.01	20.03	----	----	9.57	8.70
.08	24.94	22.69	----	----	11.49	10.46
.10	26.83	24.43	28.02	25.51	13.35	12.14
.15	31.25	28.43	----	----	17.72	16.13
.20	33.69	30.66	35.01	31.53	21.96	19.99
.30	37.42	34.05	38.23	34.79	29.41	26.76
.40	39.65	36.09	40.23	36.62	33.68	30.65
.50	41.32	37.59	42.01	38.23	36.58	33.29
.60	42.77	38.92	43.00	39.14	38.66	35.18
.70	43.94	39.99	----	----	40.39	36.76
.80	45.07	41.01	45.89	41.76	41.97	38.20
1.00	47.36	43.11	47.08	42.84	44.81	40.78
1.50	52.07	47.40	51.29	46.69	51.12	46.52
2.00	56.61	51.53	55.57	50.57	56.54	51.45
3.00	64.91	59.08	64.11	58.35	66.20	60.25
4.00	72.39	65.88	----	----	74.43	67.73
5.00	79.23	72.10	77.67	70.69	81.75	74.39

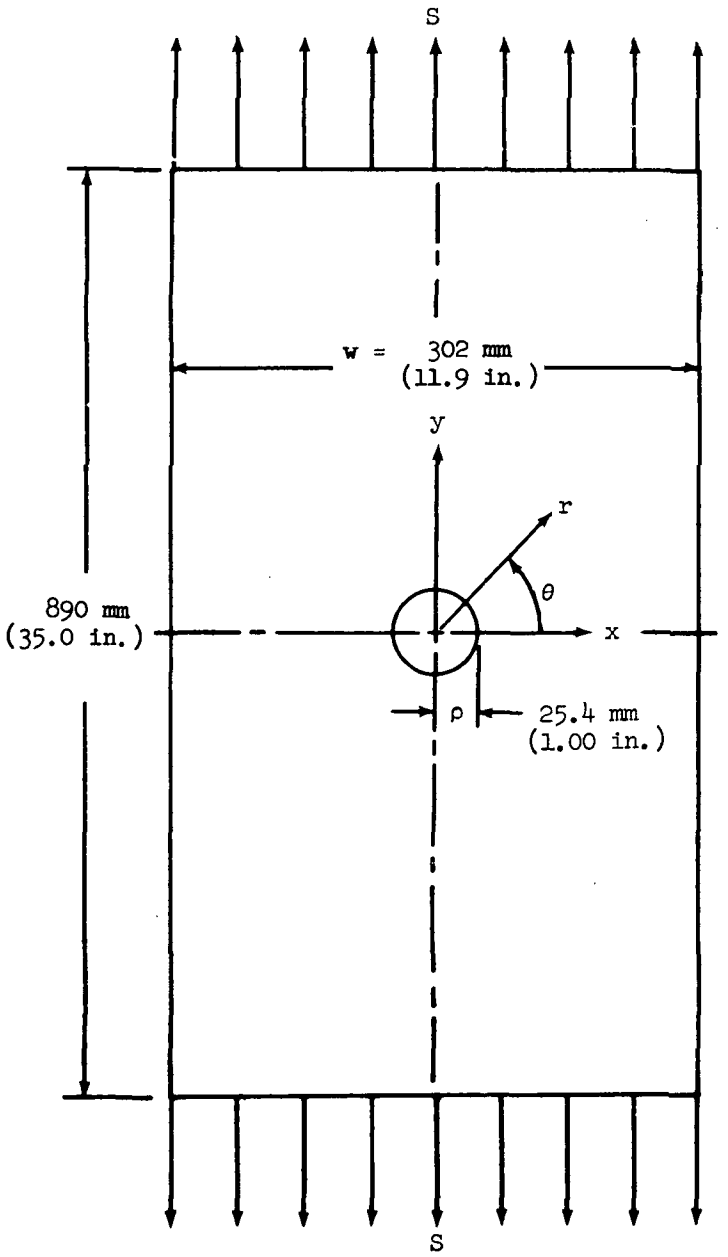

Figure 1.- Specimen configuration and dimensions. Material, 2024-T3 aluminum; thickness, 3.96 mm (0.156 in.).

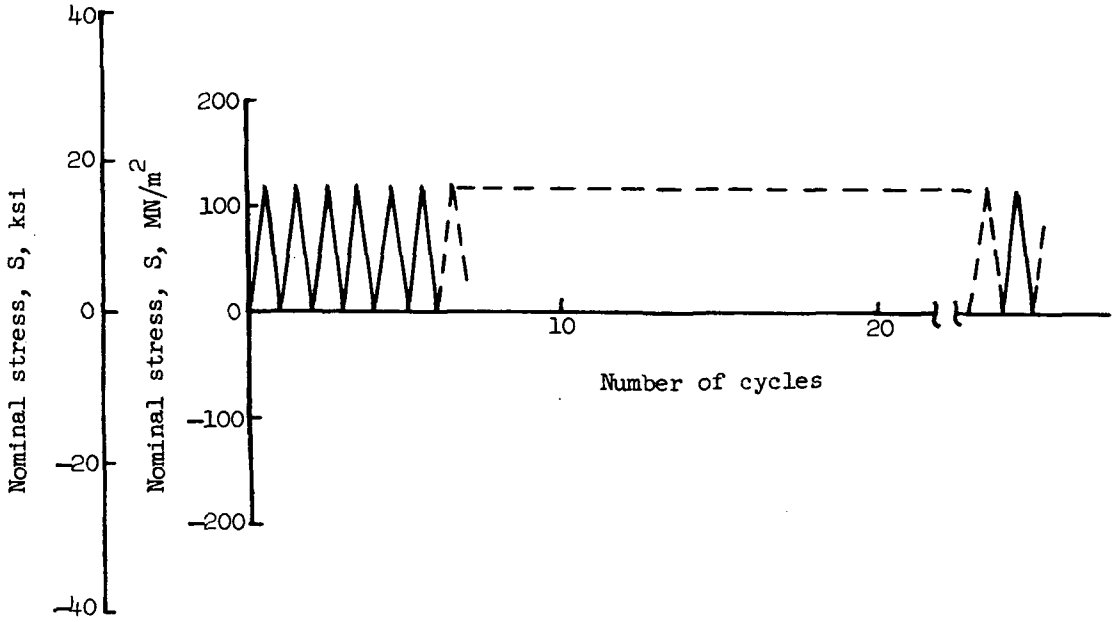

(a) Single-level loading.

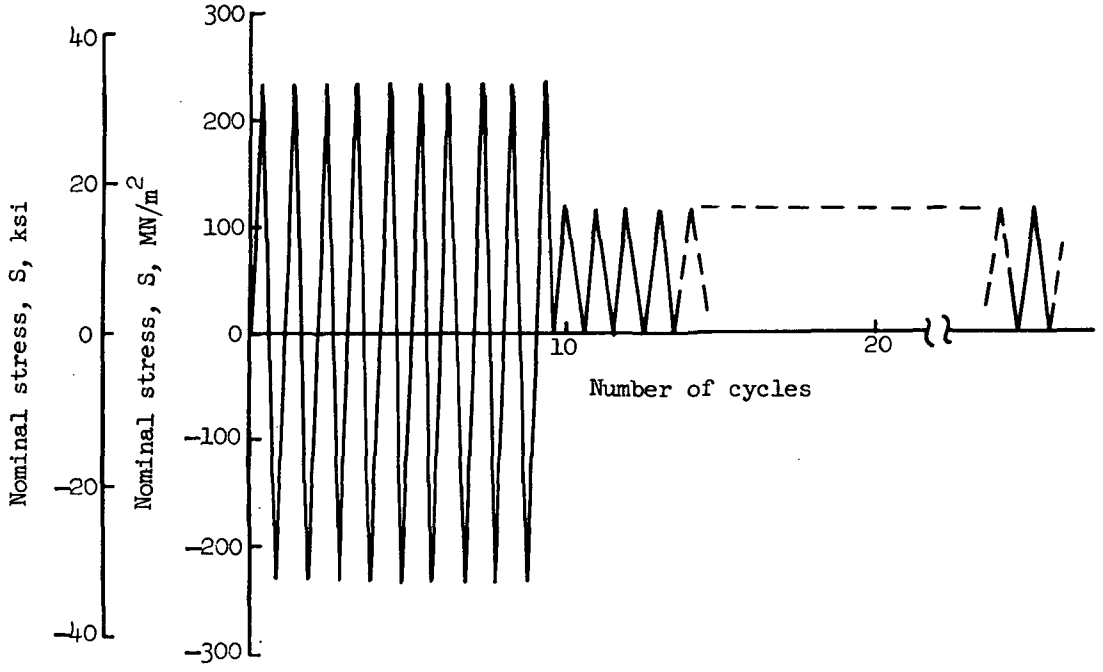

(b) Two-level loading.

Figure 2.- Loading sequences.

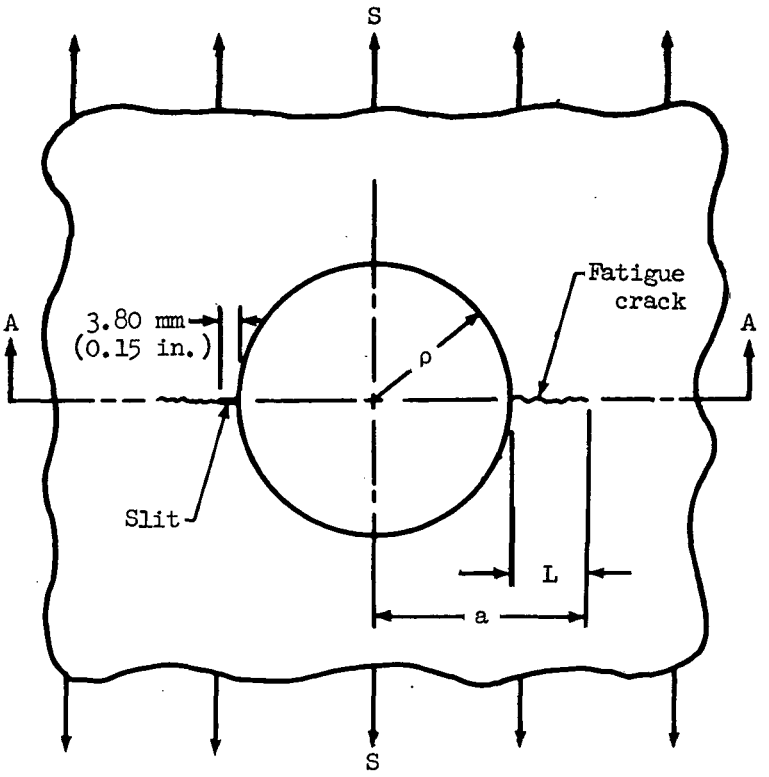

(a) Sketch showing fatigue crack and saw-cut slit.

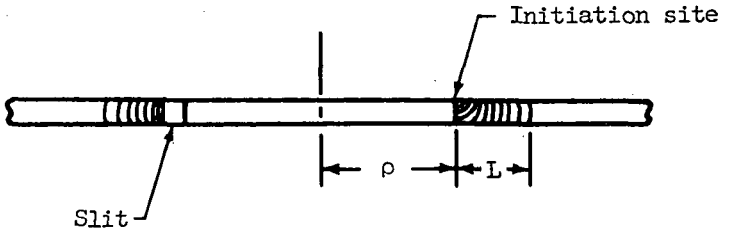

(b) Sketch of fracture surface, section A-A.

Figure 3.- Sketches illustrating fatigue crack, saw-cut slit, and fracture surface.

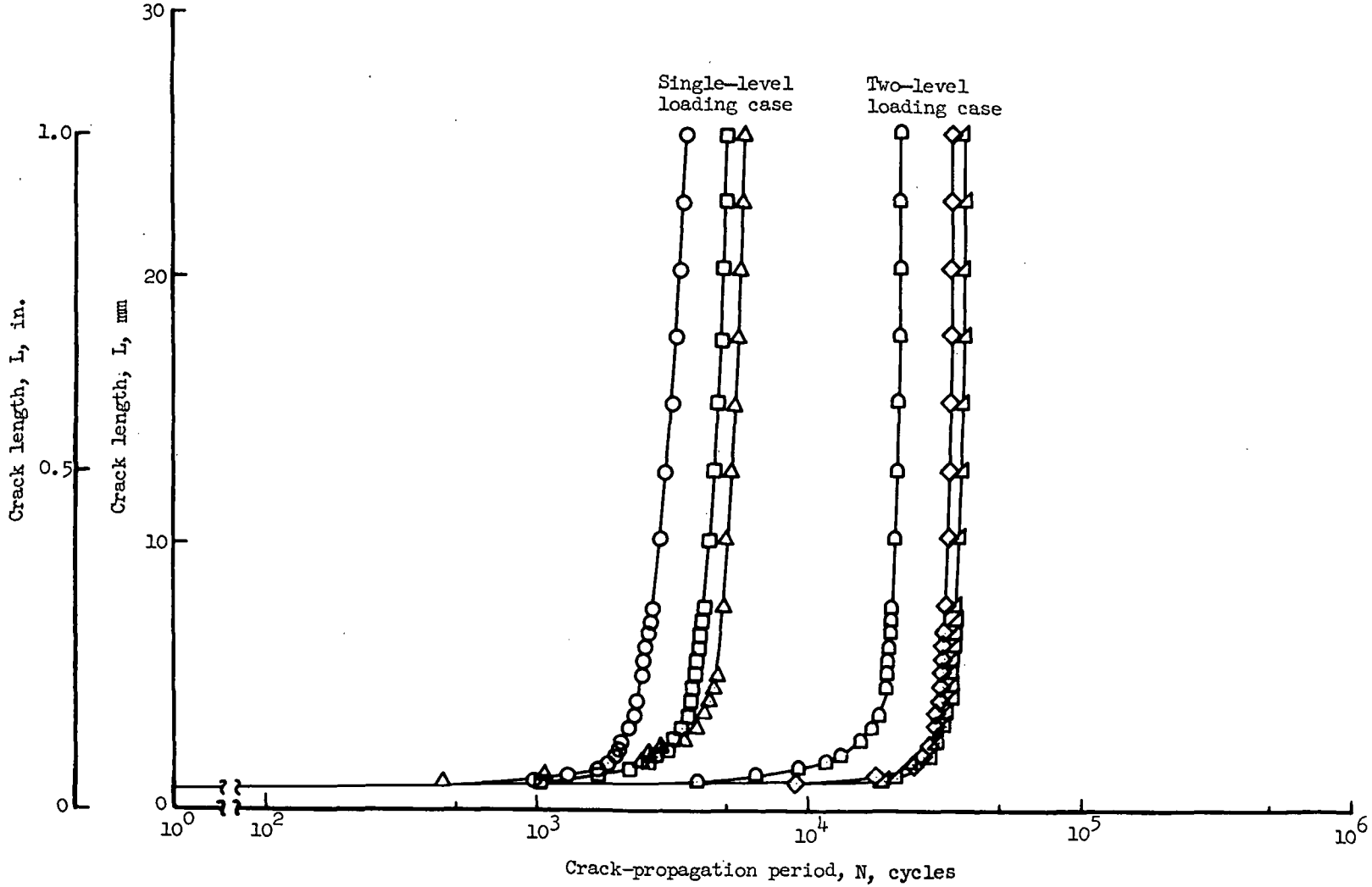

Figure 4.- Experimentally determined crack-propagation periods from table 1.

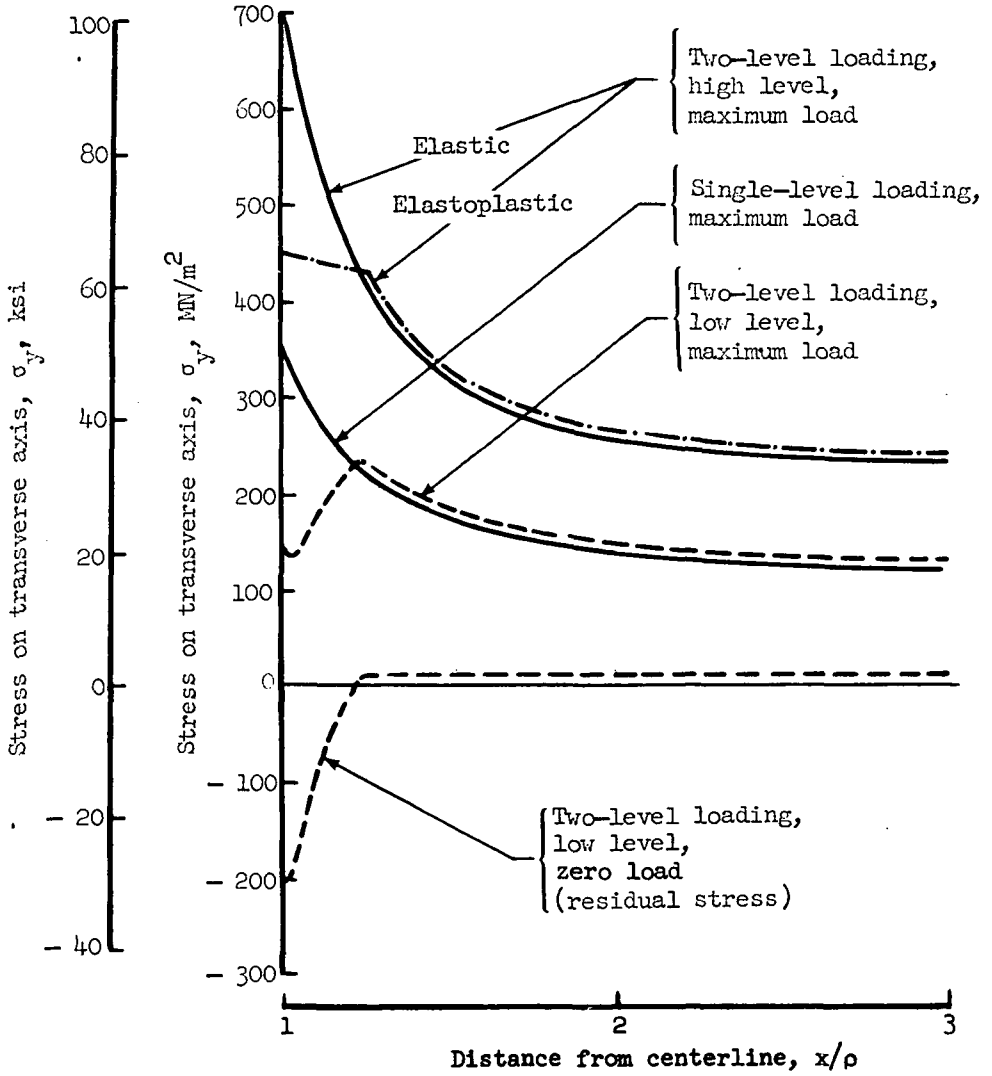

Figure 5.- Stress distributions along the transverse axis for an uncracked sheet.

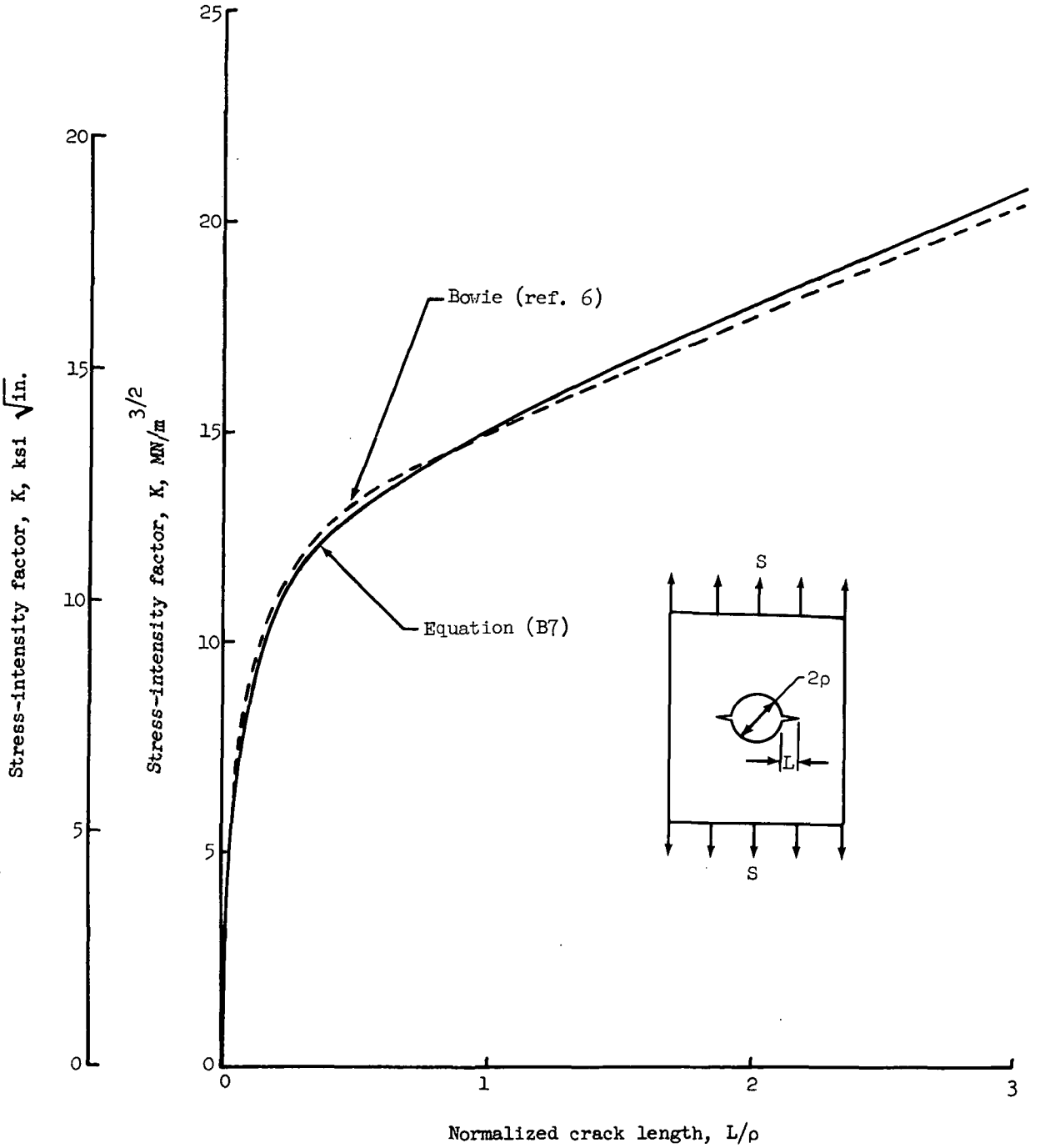

Figure 6.- Stress-intensity factors for the single-level loading case.

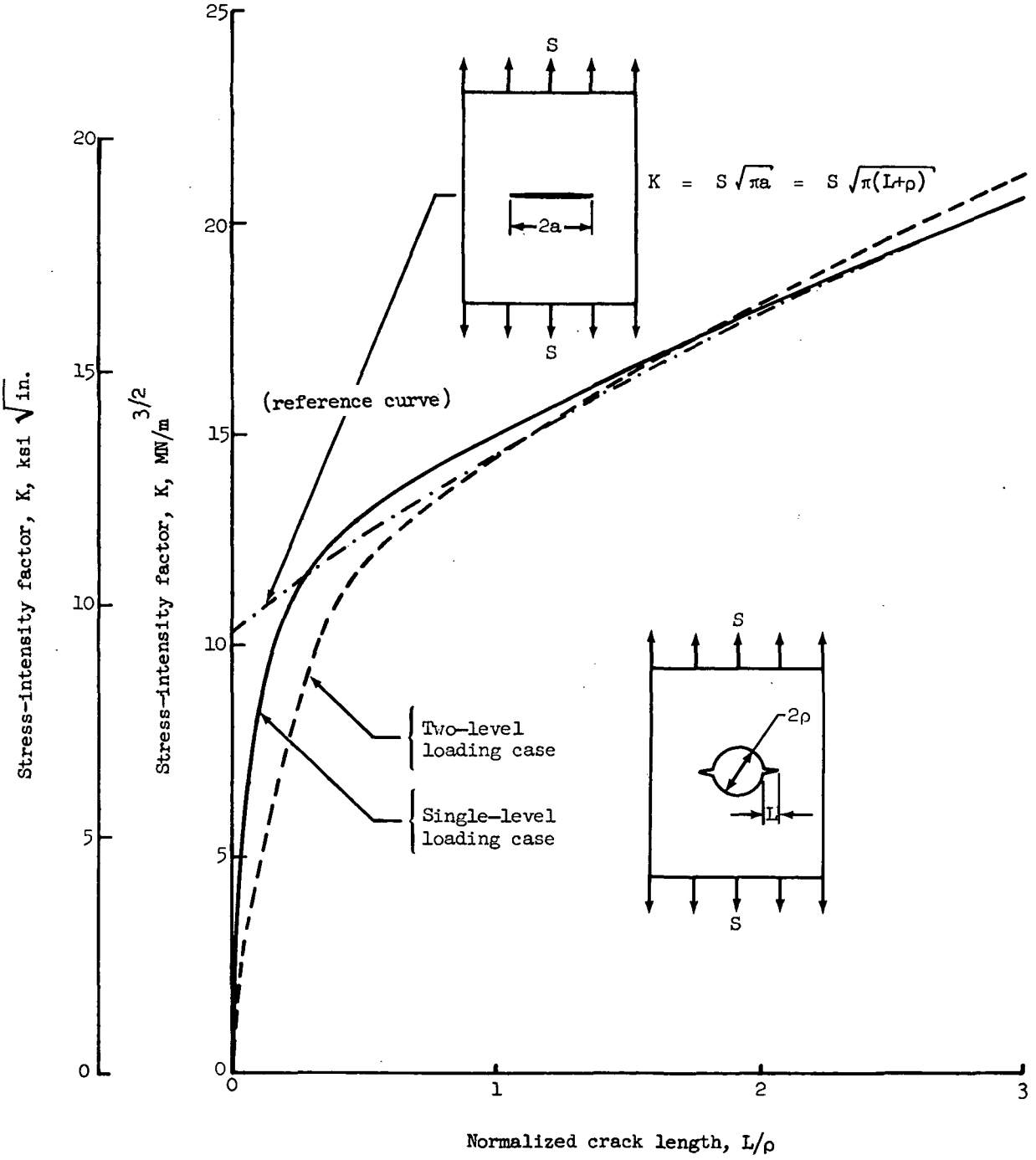

Figure 7.- Stress-intensity factors for the single-level loading and two-level loading cases.

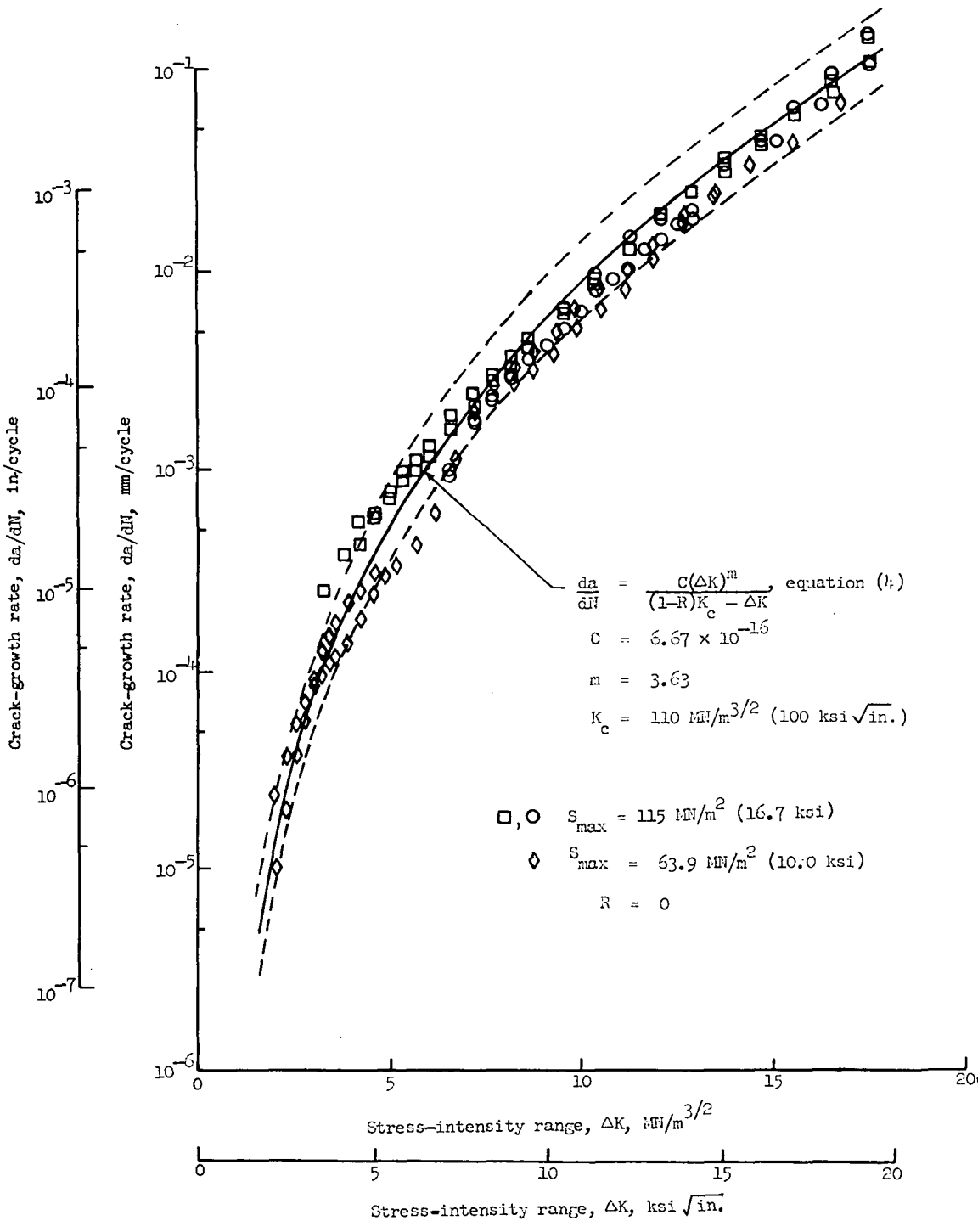

Figure 8.- K-rate curve for 2024-T3 aluminum alloy.

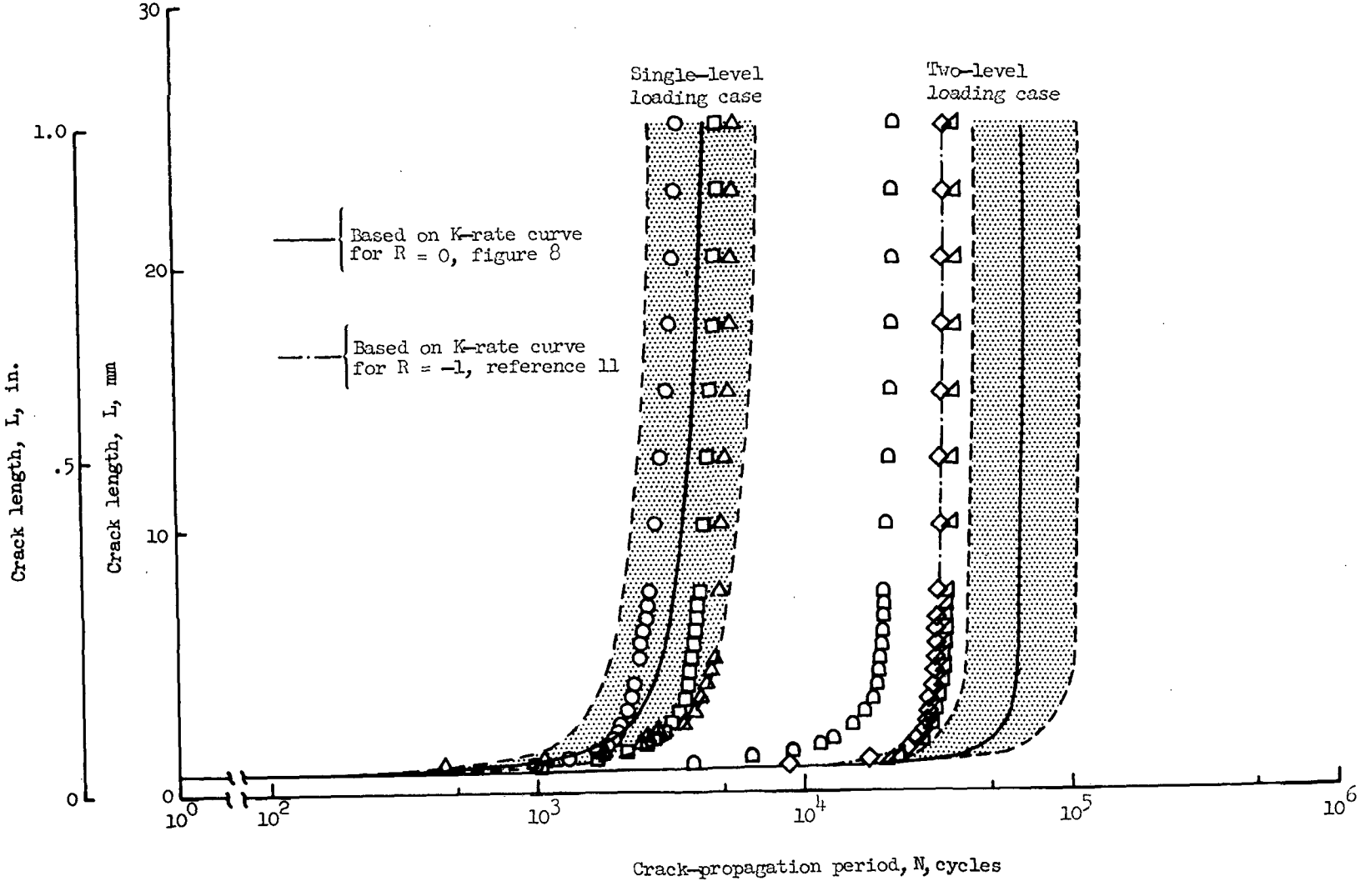

Figure 9.- Comparison of predicted and experimental crack-propagation behavior.
(Note: Shaded regions indicate predicted behavior.)

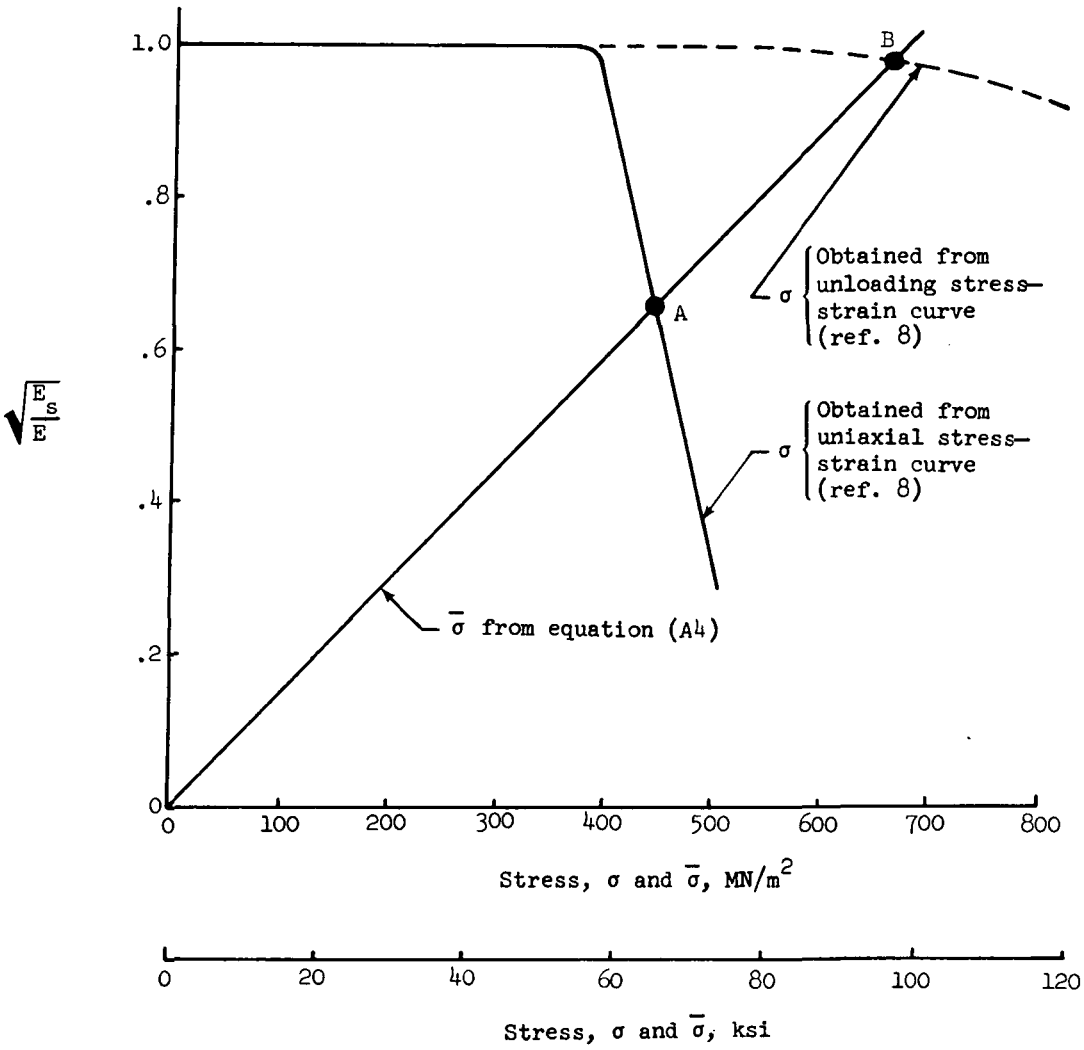

Figure 10.- Graphical procedure for obtaining $\sqrt{\frac{E_s}{E}}$.

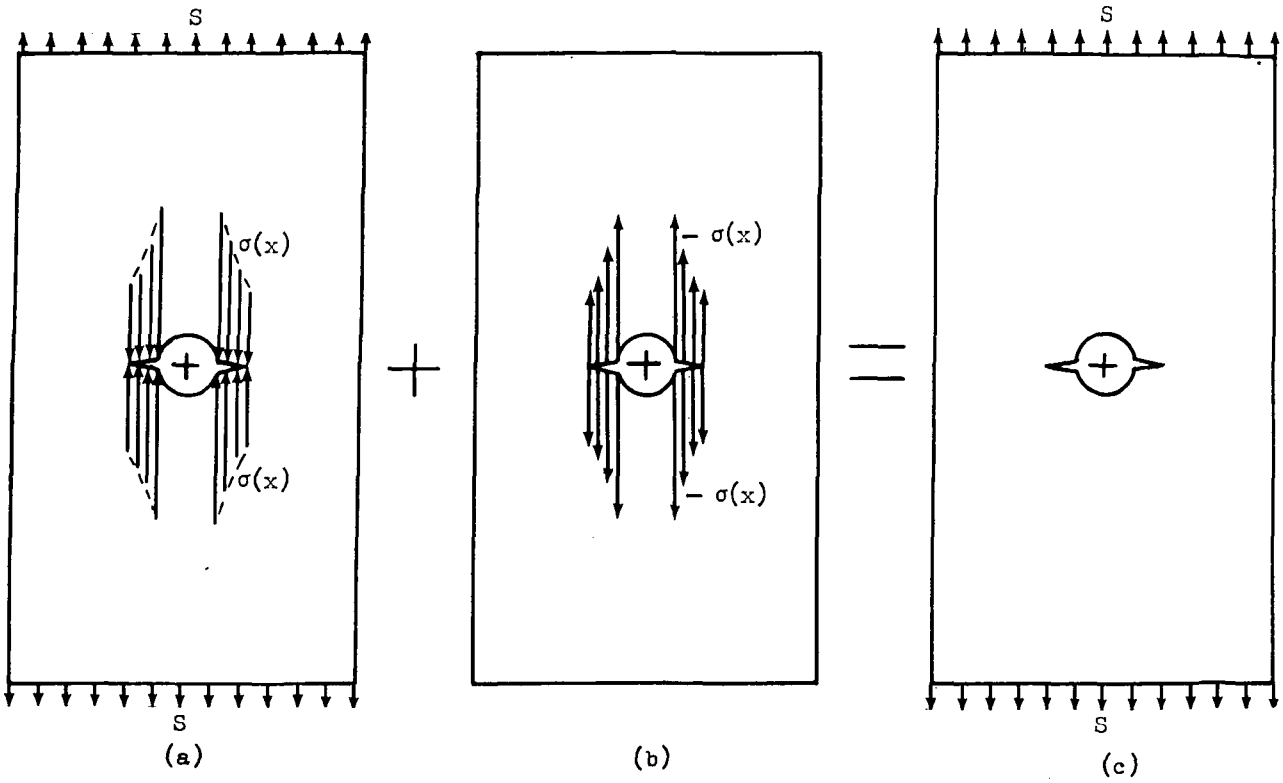

Figure 11.- Superposition of loading systems.

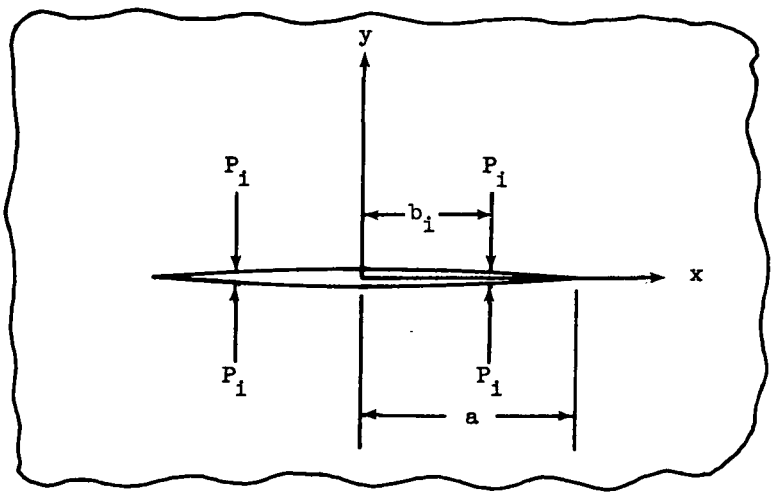

(a) Symmetrically located forces on a crack.

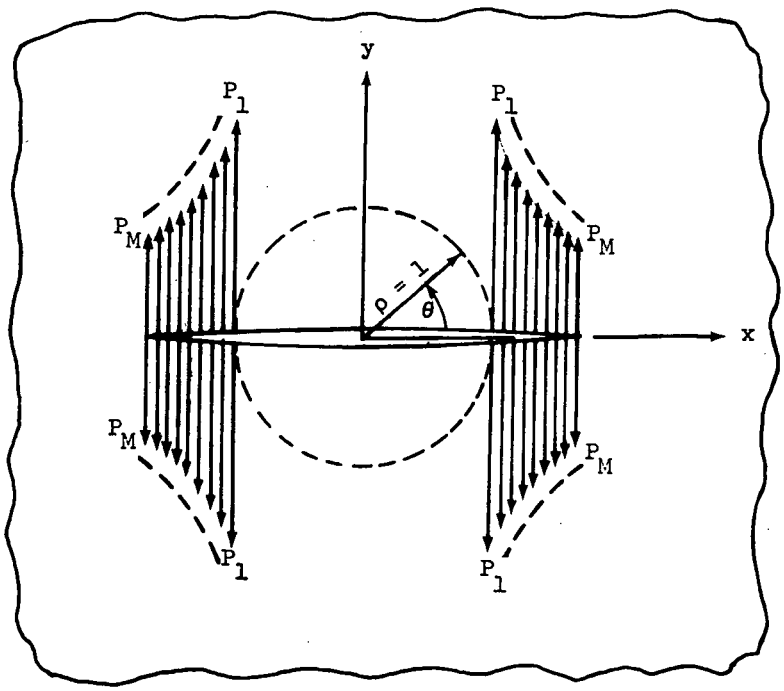

(b) System of forces used to simulate $-\sigma(x)$.

Figure 12.- Discretization of stress distribution on the crack surfaces.

NATIONAL AERONAUTICS AND SPACE ADMISTRATION
WASHINGTON, D.C. 20546

OFFICIAL BUSINESS
PENALTY FOR PRIVATE USE $300

FIRST CLASS MAIL

POSTAGE AND FEES PAID
NATIONAL AERONAUTICS AND
SPACE ADMINISTRATION

U.S.MAIL

NASA 451

POSTMASTER: If Undeliverable (Section 158 Postal Manual) Do Not Return

"The aeronautical and space activities of the United States shall be conducted so as to contribute . . . to the expansion of human knowledge of phenomena in the atmosphere and space. The Administration shall provide for the widest practicable and appropriate dissemination of information concerning its activities and the results thereof."

—NATIONAL AERONAUTICS AND SPACE ACT OF 1958

NASA SCIENTIFIC AND TECHNICAL PUBLICATIONS

TECHNICAL REPORTS: Scientific and technical information considered important, complete, and a lasting contribution to existing knowledge.

TECHNICAL NOTES: Information less broad in scope but nevertheless of importance as a contribution to existing knowledge.

TECHNICAL MEMORANDUMS: Information receiving limited distribution because of preliminary data, security classification, or other reasons.

CONTRACTOR REPORTS: Scientific and technical information generated under a NASA contract or grant and considered an important contribution to existing knowledge.

TECHNICAL TRANSLATIONS: Information published in a foreign language considered to merit NASA distribution in English.

SPECIAL PUBLICATIONS: Information derived from or of value to NASA activities. Publications include conference proceedings, monographs, data compilations, handbooks, sourcebooks, and special bibliographies.

TECHNOLOGY UTILIZATION PUBLICATIONS: Information on technology used by NASA that may be of particular interest in commercial and other non-aerospace applications. Publications include Tech Briefs, Technology Utilization Reports and Technology Surveys.

Details on the availability of these publications may be obtained from:

SCIENTIFIC AND TECHNICAL INFORMATION OFFICE

NATIONAL AERONAUTICS AND SPACE ADMINISTRATION

Washington, D.C. 20546